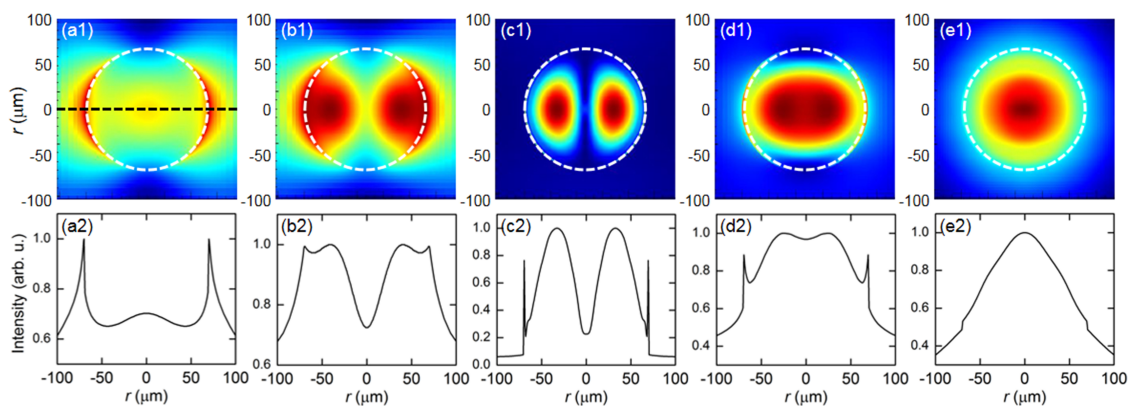


Plasma Micro-Cavity of Terahertz Wave During Laser Filamentation

Volume 11, Number 4, August 2019

Chang Liu
Yamin Chen
Jiayu Zhao
Liezhi Tang
Yan Peng
Yiming Zhu



DOI: 10.1109/JPHOT.2019.2933500

Plasma Micro-Cavity of Terahertz Wave During Laser Filamentation

Chang Liu, Yamin Chen, Jiayu Zhao , Liezhi Tang,
Yan Peng, and Yiming Zhu 

Shanghai Key Laboratory of Modern Optical System, School of Optical-Electrical and Computer Engineering, University of Shanghai for Science and Technology, Shanghai 200093, China

DOI:10.1109/JPHOT.2019.2933500

This work is licensed under a Creative Commons Attribution 4.0 License. For more information, see <https://creativecommons.org/licenses/by/4.0/>

Manuscript received July 2, 2019; accepted August 2, 2019. Date of publication August 6, 2019; date of current version August 19, 2019. This work was supported in part by Program 213 of China, in part by Shanghai Chenguang Project (18CG53), in part by National Natural Science Foundation of China (11704252 and 61722111), in part by the International Joint Lab Program supported by Science and Technology Commission Shanghai Municipality (17590750300), and in part by the Young Yangtse River Scholar (Q2016212). Corresponding author: Jiayu Zhao (e-mail: zhaojiayu@usst.edu.cn).

Abstract: In this work, we focused on the resonant cavity effect of the air plasma, formed during femtosecond laser filamentation, on the near- and far-field profiles of the generated terahertz (THz) radiation. Via the method of ray tracing, it has been demonstrated that both on-axis propagation and conical forward emission of THz wave could be qualitatively interpreted in case of considering the filament as a Fabry-Perot-like micro-cavity with radial step refractive index distribution in THz domain. Our theory might potentially solve the contradictions of different experimental observations on THz spatial profiles reported in publications, and renew the understanding of THz wave propagation inside the filament plasma column.

Index Terms: Single-color filamentation, plasma, micro-cavity, terahertz wave.

1. Introduction

The generation of terahertz (THz) wave from a single-color femtosecond laser filament in air has been studied for nearly three decades [1]–[12]. The modern view of the underlying mechanism of this THz radiation process is normally considered as the Cherenkov-type radiation [6], [7], and the forwardly emitted THz profile in the far field was detected in conical shape [6]. In this respect, the corresponding emission angle of the maximum THz lobe at one certain frequency f can be predicted via the formula of $\theta = \arcsin[c/(L \cdot f)]^{1/2}$ [6], [7], where c is the light velocity in the vacuum, and L is the filament length as the only undetermined variable. The calculated results of θ within the range of f from 0.1 to 5 THz are shown in Fig. 1, in which L was set to be 1, 3, 10 and 30 cm, respectively, according to Ref. [6]. Obviously, one can see that the higher- f THz component has a less θ , and thus would be located in the inner ring of the far-field THz donut-like profile. Besides, the overall θ decreases when L is larger.

However, the well-known transition-Cherenkov theory [6], [7] cannot well account for many other far-field THz properties in the literature, such as THz radial [2]–[5] and on-axis emission [11], or even the combination of conical and on-axis THz propagation [12], as listed in the column of “Property” in the following Table 1. Note that, these diverse properties of THz emission resulted from a similar experimental frame, i.e., single-color laser pumping THz wave generation. Actually, different profiles

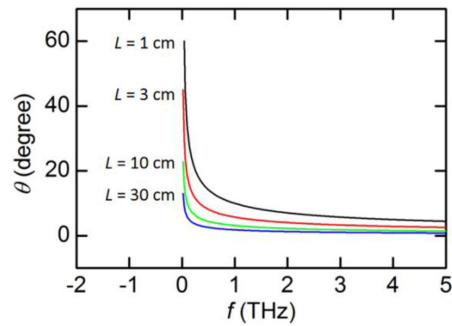


Fig. 1. The emission angle θ as a function of THz frequency f in case of four filament length L values, predicted by the transition-Cherenkov model [6], [7].

TABLE 1
THz Emission Profiles in the Far Field of a Single-Color Filament

Year	Property	Theory	Ref.
2001	Radial emission	Longitudinal plasma oscillation	[2]
2002		/	[3]
2003		/	[4]
2007		/	[5]
2007	Conical emission	Transition-Cherenkov emission	[6]
2008		Transition-Cherenkov emission	[7]
2011		Longitudinal plasma oscillation	[8]
2013		/	[9]
2018		Four wave mixing & 1D negative dielectric waveguide	[10]
2012	On-axis propagation	Parametric decay	[11]
2013	Conical & on-axis propagation	Electric quadrupoles	[12]

of THz radiation appeared, even if the adopted initial parameters of the experiments were almost the same [5], [6].

On the other hand, various mechanisms (column “Theory” in Table 1) were proposed to describe the above different experimental results of the far-field THz patterns, e.g., longitudinal plasma oscillation [2], [8]. Besides, transverse plasma oscillation [13] and both longitudinal and transverse plasma oscillations [14] have also been suggested. However, a common origin has not been achieved, to the best of our knowledge, in order to be responsible for all these complicated and inconsistent observations.

Note that THz pulses are generated from the inside of the filament, nevertheless the influence of the air-plasma interface on THz wave propagation and the corresponding spatial distribution modulation have long been neglected. Recently, it has been discovered that the filament plasma not only plays the role of a THz wave generator, but also acts as a THz waveguide due to the post-stage interaction between the free electrons and the generated THz wave. This effect has been observed as the phenomenon of spectral self-action [15] or spatial confinement [16], [17] in the THz spectral region.

Thus in this work, attentions have been paid to the waveguide effect of the air plasma on the THz radiation during filamentation. Specifically following the concept of spatial confinement of THz wave, a plasma-formed THz micro-cavity model has been built. It has been proved that the filament could form a resonant micro-cavity in THz band, which possesses the capability of creating radial and conical or even on-axis THz beam radiations. Accordingly, the previously reported THz far- and

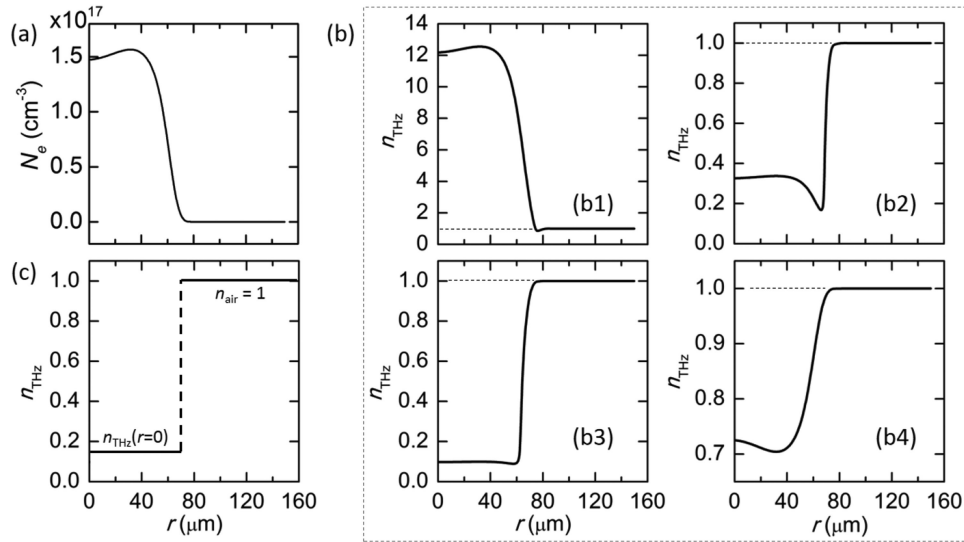


Fig. 2. (a) The simulated radial N_e distribution [18]. (b1-b4) Four examples of n_{THz} calculated at 0.1, 1, 2 and 5 THz, respectively. (c) The simplified evolution of n_{THz} along r .

near-field properties in the literature could be interpreted by the modulation of the micro-cavity's step-index on the guided THz wave.

2. Theory and Analytical/Numerical Calculations

2.1 Radial Refractive Index Distribution of the Filament in THz Band

In order to investigate the possibility of a filament being a waveguide of THz wave, it is essential to obtain the information of the plasma density N_e distribution within the filament area. Here, the characteristic radial distribution of N_e in the cross section of the filament has been borrowed from our previous work (Ref. [18]), and redrawn in Fig. 2(a). It was simulated at the geometrical focus of the lens, based on the nonlinear wave equation using the slowly varying envelop approximation [19]. More detailed information could be found in Ref. [18]. Impressively, this N_e distribution has an off-axis maximum, which has been experimentally confirmed by Ref. [20]. This structure has also been tested to be appropriate for guiding laser pulses or even x-ray during filamentation [21], [22]. Thus, one will be curious about whether it still works for THz waves.

The corresponding n_{THz} distribution of the filament in THz band can be given by the real part of the square root of the permittivity (relative dielectric constant ϵ_r):

$$n_{\text{THz}} = \text{Re}(\sqrt{\epsilon_r}) = \text{Re}\left(\sqrt{1 - \frac{\omega_p^2}{\omega^2 - i\nu\omega}}\right), \quad (1)$$

where ν is the free electron collision frequency (typically at 1 THz [23]); ω is the THz angular frequency ($\omega = 2\pi f$); and ω_p indicates the plasma frequency (in SI units):

$$\omega_p = \sqrt{\frac{e^2}{m_e \epsilon_0} N_e}. \quad (2)$$

e represents the electric charge, and m_e indicates the effective mass of the electron, and ϵ_0 is the permittivity in the vacuum. Four representative results of n_{THz} , calculated at $f = 0.1, 1, 2$ and 5 THz, are shown in Fig. 2(b1-b4), respectively. One can see that n_{THz} has a common feature of a step change at around $r = 70$ μm (nearly half of the filament diameter), and then its value approaches 1 towards the periphery of the filament (air region). In view of the radial step of n_{THz} , as well as its

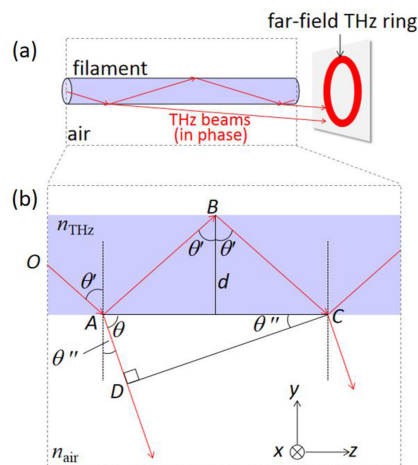


Fig. 3. (a) The diagram of THz beam propagation path along the filament and the expected far-field THz ring. (b) The detailed THz beam paths in the y - z plane inside the plasma column.

relative flatness evolutions on both sides of the sharp change, it is reasonable to simplify n_{THz} to the one as shown in Fig. 2(c). That is, the value of n_{THz} is set to be a constant as $n_{THz}(r=0)$ or 1, inside or outside the step change, respectively. In this case, the filament is a homogeneous index rod in the THz spectral region with diameter smaller than (or comparable with) the THz wavelength. Accordingly, the parallelism of the air-plasma interfaces becomes intrinsically excellent, so that the radial oscillation of THz wave inside the filament column can no longer be ignored.

In the following sections, based on the simplified radial n_{THz} distribution [Fig. 2(c)], THz modes formed in the far field of the filament and inside the plasma channel have been analytically solved and numerically simulated with a simple resonant micro-cavity model. By developing the method of “ray tracing”, which has already been successfully used in field of Fabry-Perot (F-P) micro-cavity analysis [24], [25], it has been demonstrated that, as for a filament with diameter comparable with the THz wavelength, the transmission and reflection of the THz wave at the air-plasma interface are strongly dependent on the intrinsic F-P nature of this filament based THz micro-cavity.

It is also worth mentioning that, it has been suggested that the THz generation is mainly at the front of a femtosecond laser pulse and is thus almost not affected by the plasma [26]. This seems to disagree with the precondition of this work: interactions between the plasma and THz wave occur inside the filament channel. As for this issue, however, the authors from the same joint research group of Ref. [26] later theoretically confirmed that the generated THz pulse had an interaction with the air plasma as the post-process after its generation, which inevitably led to the THz spectral self-action (broadening) [15]. Recently, this effect has been experimentally clarified as the spatial confinement of THz wave inside the plasma column [10], [27].

2.2 Frequency-Dependence Emission Angle of the Far-Field THz Mode

It is well known that the plasma could be produced within the same temporal scale of the pumping laser pulse duration, e.g., a few tens of femtoseconds [28], while the plasma’s average lifetime is as long as several nanoseconds [29]. In contrast, the building time of the THz pulse is around a few picoseconds, much longer than that of the plasma, but much shorter than the plasma’s lifetime. This fact hints that, the plasma could be formed in an instant moment before the THz pulse generation. Afterwards, it would last enough long time for guiding the THz wave inside it. For this reason, the plasma channel can be treated as a static THz waveguide.

Assume that the THz wave, emitted from the origin o inside the filament plasma column, propagates in all directions. Then the following multiple THz refractions and coherent combinations could make a far-field THz mode, which are schematically shown in Fig. 3(a). Here, the problem that we

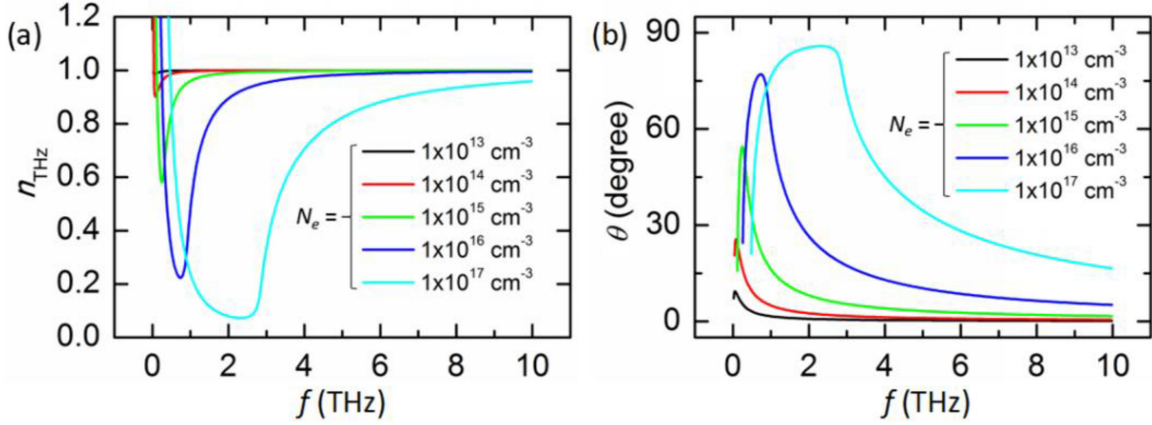


Fig. 4. (a) n_{THz} as a function of THz frequency f at different N_e values from 10^{13} to 10^{17} cm^{-3} . (b) The corresponding THz radiation angle θ .

considered in this paper is a pure one-dimensional problem, thus the diffraction effect has been neglected [24], [25].

In Fig. 3(b), more details have been introduced in the y - z plane. Our central concern of THz radiation angle θ , in direction of which the THz pulses achieve constructive interference in the far field, can be deduced as follows. Firstly, the optical path difference Δ between two adjacent refracted THz beams is given by

$$\Delta = n_{THz}(AB + BC) - n_{air}(AD) = 2 \frac{d}{\cos \theta'} (n_{THz} - n_{air} \sin \theta' \sin \theta'), \quad (3)$$

where d is the diameter of the filament cylinder, and θ' is the incidence angle of THz ray on the plasma-air interface, and θ'' is the refractive angle in the air side (also the complementary angle of θ). Moreover, at the plasma-air interface, the THz wave follows the Snell's law: $n_{THz} \sin \theta' = n_{air} \sin \theta''$, which can be substituted into Eq. (3), and one would thus obtain

$$\Delta = 2n_{THz}d \cos \theta'. \quad (4)$$

Secondly, if considering the constructive coherence of THz wave in the far field, the optical path difference Δ should be an integral multiple of the THz wavelength λ_{THz} , thus $\Delta = m\lambda_{THz}$, where m is any natural number. Hence, it is clear that

$$m\lambda_{THz} = 2n_{THz}d \sqrt{1 - \left(\frac{n_{air} \cos \theta}{n_{THz}} \right)^2}. \quad (5)$$

At last, by solving the above Eq. (5), the expression of θ is as follows (Appendix):

$$\cos \theta = \sqrt{\frac{(2n_{THz}d)^2 - (m\lambda_{THz})^2}{(2n_{air}d)^2}}. \quad (6)$$

As for the zero order of $m = 0$:

$$\cos \theta = \frac{n_{THz}}{n_{air}} \approx n_{THz}. \quad (7)$$

It is worthy of noting that, the THz wave emission from a single-color filament has been demonstrated to be radially polarized in a conical shape [6], i.e., a typical TM-like mode. According to this fact, on the plasma-air interface, the phase change (e.g., ϕ) of the Fresnel reflection coefficient is always 0 or π , as long as n_{THz} is smaller than n_{air} [30]. Since this condition can be easily fulfilled in view of the coming Fig. 4(a), the phase difference between two adjacent THz beams in the far field (i.e., 2ϕ) would be 0 or 2π , which thus could be neglected during calculations of Δ .

In addition, by reading Eq. (7), it is interesting to find that θ depends solely on n_{THz} . While in the formula of n_{THz} [Eq. (1), (2)], N_e is the only undetermined variable, besides the THz angular frequency $\omega = 2\pi f$. In the next step, N_e value has been varied to study the evolutions of n_{THz} and θ . The calculated results given by Eq. (1) and (7) are shown in Fig. 4(a) and (b), respectively.

It can be seen in Fig. 4(a) that n_{THz} is larger than 1 in the low-frequency band (mostly around 0.1 THz). This might account for the well-known Cherenkov-type radiation of THz wave [6], whose propagation velocity must be smaller than that of the oscillating electron driven by the laser intensity with velocity of c . Afterwards, in Fig. 4(a), n_{THz} decreased to the minimum due to the resonance between THz wave and the plasma ($\omega_{THz} = \omega_p$) [16]. Then, n_{THz} gradually increased and finally approached the unity. Overall, n_{THz} of the filament is mainly below the unity. Coincidentally, in view of Eq. (7), only $n_{THz} < 1$ can result in a solvable θ . Hence, the filament is very likely to be an ideal waveguide for THz wave.

This issue has been further confirmed by Fig. 4(b), in which θ basically decreased with the increasing f , hinting that the higher-frequency THz component preferred a smaller angle in order to achieve constructive coherence and form a far-field THz ring. This calculation result of θ has the similar tendency with Fig. 1 predicted by the Cherenkov model [6], [7], and also with Fig. 8 in Ref. [10] simulated by the 1DND model. Moreover, as for one certain THz frequency, its θ increased with the increasing N_e . This observation is in accordance with Fig. 4 in Ref. [6], in which L was decreased together with the increasing of N_e by shortening the focal length of the lens [31].

Moreover, in case of $f \gg \nu$, Eq. (7) could be further deduced as

$$\cos \theta \approx n_{THz} = \text{Re} \left(\sqrt{1 - \frac{\omega_p^2}{\omega^2 - i\nu\omega}} \right) \approx \sqrt{1 - \frac{\omega_p^2}{\omega^2}}. \quad (8)$$

Thus

$$\sin \theta \approx \frac{\omega_p}{\omega}. \quad (9)$$

Since ω_p is proportional to $N_e^{1/2}$ as shown in Eq. (2) and $\omega = 2\pi f$, then

$$\theta \propto \arcsin \frac{\sqrt{N_e}}{f}. \quad (10)$$

The simplified outcome above is consistent with the result as shown in Fig. 4(b) towards high THz spectral region. Compared with $\Delta = \arcsin[c/(L \cdot f)]^{1/2}$ determined by the quasi-Cherenkov radiation in Ref. [6], [7], these two expressions are associated with each other by $N_e \sim 1/L$, which is supported by Ref. [31], [32]. This mathematical coincidence between two formulas actually indicates that, the plasma micro-cavity model suggested in this work might be another possible way for THz wave phase matching during propagation (besides the Cherenkov scheme [6]), following the THz generation stage driven by the longitudinal ponderomotive forces for one-color plasma [1].

It has also been reported that the resonant THz transition radiation could be generated at two sharp plasma-vacuum boundaries driven by a normally incident laser pulse [14], [33], [34]. However, it is obviously not our case, since the considered plasma-air interfaces in this paper between which THz waves oscillated were parallel to the laser propagation direction.

Till now, the f -dependent conical THz emission in the far field has been theoretically reproduced. Another important phenomenon of the reported THz radial radiation as shown in Table 1 will be investigated in the next Section 2.3. And the related numerical simulations have been performed in Section 2.4. Moreover, it can be noticed that in the region from $n_{THz} = 1$ to $n_{THz} = \text{minimum}$ [Fig. 4(a)], the corresponding θ increased with the increasing THz frequency [Fig. 4(b)], against the overall trend of θ - f . This issue will be briefly discussed in Section 2.5.

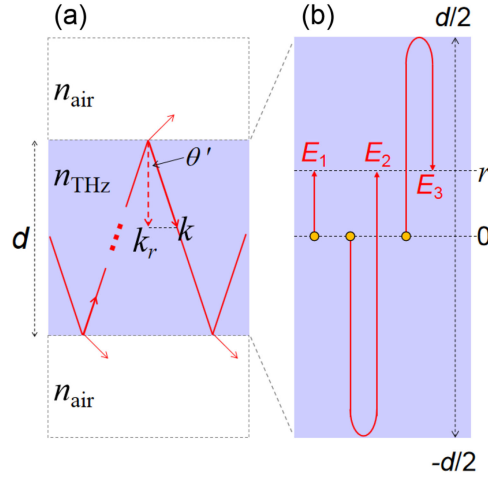


Fig. 5. (a) A longitudinal slice of the simplified model of a filament with homogeneous refractive indices of n_{THz} (inside) and n_{air} (outside). (b) Partially enlarged details of THz wave radial oscillations inside the filament slice.

2.3 Near-Field THz Modes Inside the Plasma Column

The above Section 2.2 dealt with the multiple refractions of THz wave at the periphery of the filament cylinder, which resulted in far-field THz modes. In this section, multiple reflections during THz wave propagation inside the plasma column have been investigated instead. Although a more precise 1DND model has been built in Ref. [16], the formation process of the ring-shaped THz propagation mode is still unclear. Thus, the following deducing is aimed at uncovering the basic physics of this phenomenon.

Noting that along the plasma channel, the THz energy loss could be compensated by the gain acquired during the filamentation [18], here we solely concentrated on one longitudinal slice of the filament, as shown in Fig. 5(a), which was cut from the plasma micro-cavity in Fig. 3(b). All the following calculations on THz oscillations are made in the radial direction of this filament slice.

Once again, the simplified distribution of n_{THz} as shown in Fig. 2(c) was employed, and the radial diameter of the plasma zone was written as d [Fig. 5(a)], from $-d/2$ (one end) to $+d/2$ (the other end) by taking the center as the origin zero [Fig. 5(b)]. The THz wave with amplitude of E_0 was assumed to be emitted from the origin line, and the THz electric field $E(r)$ at a certain radial distance of r from the origin line can be calculated as

$$E(r) = \sum_{i=1}^3 E_i \sum_{N=0}^{\infty} \{R^2 \exp[i(k_r \cdot 2d + 2\phi)]\}^N, \quad (11)$$

where E_i ($i = 1, 2$ and 3) represents the amplitudes of three different THz rays reaching the location r [Fig. 5(b)].

As for the first one, E_1 is the amplitude of the THz ray which was emitted from the origin line to reach the point r directly without any reflection on the air-plasma interfaces:

$$E_1 = E_0 \exp[i(k_r \cdot r)]. \quad (12)$$

Thus, there is a phase shift of $k_r \cdot r$ between E_1 and E_0 , where $k_r = k \cdot \cos\theta' = (2\pi \cdot n_{\text{THz}} \cdot f/c) \cdot \cos\theta'$ is the transverse component of THz wave vector k , and θ' is the angle between k and k_r , i.e., the THz incidence angle on the air-plasma interface. In the same manner, the second one, E_2 , is the amplitude of the THz ray which was emitted from the origin line to reach the same position r , however, via one additional reflection:

$$E_2 = R \cdot E_0 \exp\{i[k_r \cdot (d + r) + \phi]\}. \quad (13)$$

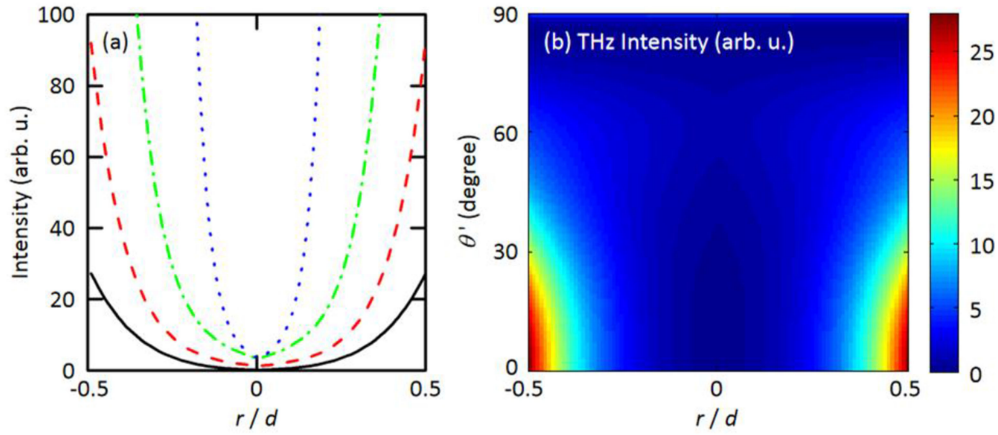


Fig. 6. (a) Distributions of the THz mode field intensity $I(r)$ at λ_n/d of 2 (black solid line), 1.5 (red dashed line), 1 (green dash-dot line) and 0.5 (blue dotted line), respectively. (b) Near-field THz propagation modes at $\lambda_n/d = 2$ with respect to θ' (0–90 degree).

Here, R is the reflection coefficient of the THz ray at the air-plasma interface, and $\phi = 0$ or π is the corresponding phase shift, both of which followed Fresnel's equations for TM wave [30]. At last, E_3 is the amplitude of the 3rd THz ray which was emitted from the origin line, passed the position r , reflected on the interface and then returned back to r :

$$E_3 = R \cdot E_0 \exp\{i[k_r \cdot (d - r) + \phi]\}. \quad (14)$$

Moreover, each E_i is considered experiencing infinite round trips inside the cavity given by the item of $\sum_{N=0}^{\infty} \{R^2 \exp[i(k_r \cdot 2d + 2\phi)]\}^N$ [the latter half of Eq. (11)], in which $k_r \cdot 2d$ is the phase shift induced by one round trip inside the filament cavity, and $2\phi = 0$ or 2π is introduced by the reflections on both interfaces at $+d/2$ and $-d/2$. If further taking into account of the infinite series of $\sum_{N=0}^{\infty} \{R^2 \exp[i(k_r \cdot 2d + 2\phi)]\}^N = \frac{1}{1 - R^2 \exp[i(k_r \cdot 2d + 2\phi)]}$, finally, $E(r)$ in Eq. (11) can be computed by

$$E(r) = E_0 \frac{\exp[i(k_r \cdot r)] + R \exp\{i[k_r \cdot (d + r) + \phi]\} + R \exp\{i[k_r \cdot (d - r) + \phi]\}}{1 - R^2 \exp[i(k_r \cdot 2d + 2\phi)]}. \quad (15)$$

Then, the THz mode field intensity $I(r)$ can be calculated by multiplying $E(r)$ with its conjugate item, i.e., $I(r) = E(r) \cdot E^*(r)$. Four examples of $I(r)$ are shown in Fig. 6(a). It can be seen that $I(r)$ has maximums at the interfaces ($r = \pm d/2$), which well agrees with the mode profiles given by calculations and simulations in Ref. [16], [18].

As shown in Fig. 6(a), $I(r)$ was calculated by setting λ_n/d as four different values (i.e., 2, 1.5, 1 and 0.5), where $\lambda_n = \lambda/n_{\text{THz}}$ is the THz effective wavelength inside the plasma column. And the used reflection coefficient R at the interface was about 0.33 given by Fresnel's equations. $\lambda_n/d = 2$ actually corresponds to the case of $f = 0.1$ THz as shown in Fig. 2(b1), and $\lambda_n/d = 0.5$ denotes that of $f = 5$ THz in Fig. 2(b4). The decreasing of λ_n/d (from 2 to 0.5) is in fact equivalent to the increasing of the THz frequency. It can be seen that the higher-frequency THz mode has the smaller "opening" (ring diameter), which agrees with the variation trend predicted by the 1DND model [16]. This result is also not in contradiction with the far-field outcomes as shown in Fig. 1 (quasi-Cherenkov model) or Fig. 4(b), if considering the diffraction of the f -related in-cavity THz mode (Fig. 6(a)) at the end of the filament into air.

In addition, in the above calculations of $I(r)$ as plotted in Fig. 6(a), θ' was set to 0 for the sake of convenience. Next, θ' was varied from 0 to 90 degree and the corresponding $I(r)$ results with λ_n/d fixed at 2 are shown in Fig. 6(b). One can see in Fig. 6(b) that the ring-shaped THz propagation mode was obtained mainly at $\theta' = 0$ degree, which reveals that the formation of strong THz in-cavity mode depends on the normal incidence of THz wave onto the $n_{\text{THz}} - n_{\text{air}}$ interface. This coincides the theory of THz wave radial emission [2]–[5], which could be the origin of THz oscillations inside

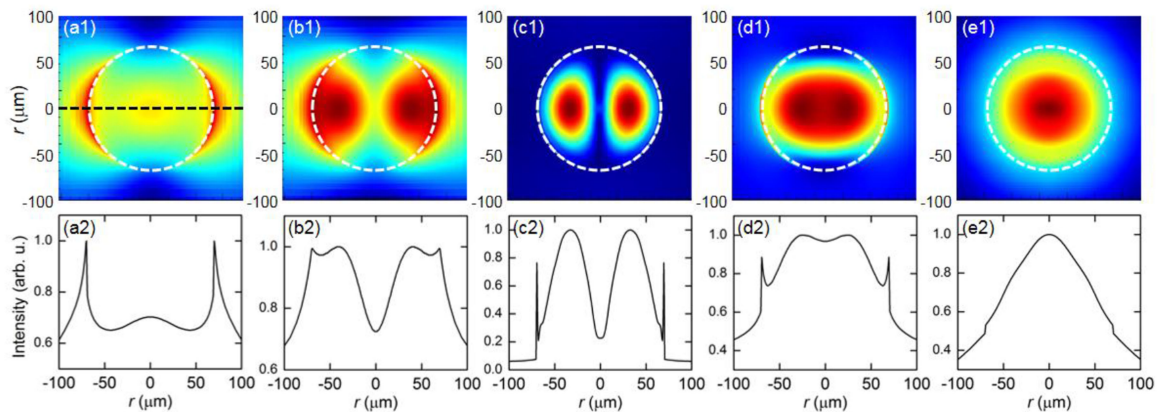


Fig. 7. (a1-e1) The simulated THz modes within the cross section of the filaments at 0.1, 1, 2, 5 and 10 THz, respectively. (a2-e2) The corresponding radial distributions of the THz mode intensity.

the plasma column. During this oscillation, multiple THz refractions and reflections occurred (Fig. 3 and 5), thus the far- and near-field THz modes finally came into being (Fig. 4 and 6).

Compared with the far-field THz mode, the THz propagation mode inside the filament could be much less in intensity. This is due to the fact that the reflection coefficient R on the interface for a TM-polarized THz mode [16], [18] normally has a small value, e.g., 0.33 used in Fig. 6, in case of n_{THz} (inside) being smaller than n_{air} (outside) [30]. In practice, one has to eliminate the far-field THz mode in order to observe the diffraction of the near-field one [35].

2.4 Numerical Simulations of the THz Propagation Mode

In order to further confirm our theory, in this section, numerical simulations have been performed to study the possible THz modes inside the cross section of the filament. By inputting the simplified distributions of n_{THz} , as shown in Fig. 2(c), into a commercial software *FDTD Solutions*, THz eigenmodes localized in the filament area have been established by the finite-difference time-domain (FDTD) method.

Fig. 7(a1-e1) show the intensity profiles of these modes at 0.1, 1, 2, 5 and 10 THz, respectively. Since the fields are identical after a rotation of $\pi/2$ radian, only one of the doublet degenerated modes is illustrated. It can be seen that the THz energy is strongly constrained inside a circular region (white dashed circle) which marks the trajectory of the radial step change of the index distribution as shown in Fig. 2(c). To begin with, in low THz band (Fig. 7(a1)), most of the energy is located at the interface between the plasma and the air. However, with the growth of THz frequencies, the mode field tends to converge to the cross-sectional center (Fig. 7(e1)). Fig. 7(a2-e2) further display the corresponding radial distributions of the mode intensity at each THz frequency along the black dashed line as indicated in Fig. 7(a1). One could clearly see the evolution of the modal ‘opening’ which decreased with the increasing THz frequency, in accordance with the calculated ones (Fig. 6(a)).

2.5 Resonant Cavity Effect of the Filament in Two-Color Case

In the above sections, the micro-cavity effect of the single-color filament on the generated THz wave has been discussed. In practice, a two-color laser field pumping scheme [36] is often chosen in order to further increase the THz yield. The micro-cavity effect of the filament in principle could also be applicable in the situation of two-color photoionization in air, as long as the created THz wave has a radial component inside the plasma column (Fig. 5). Therefore in this section, we attempted to extend our resonant cavity theory to the two-color case, aiming at qualitatively interpreting the

TABLE 2
THz Emission Profiles in the Far Field of a Dual-Color Filament

Property	Relationship	Ref.
Conical emission (ring diameter versus THz frequency)	Anti-correlation	[37-40]
	Non-correlation	[41]
	Positive-correlation	[32]
On-axis propagation with bell-shaped profile	/	[35,42,43]

potential reasons of diverse THz profiles observed in dual-color laser pumping THz generation experiments [32], [35], [37]–[43].

It is well known that THz wave diffracts in a smaller angle with the increase of its frequency during two-color filamentation [37]–[40]. This nature has been explained by the off-axis phase matching model [37]. However, when the length of the filament is smaller than the dephasing length (~ 22 mm for a filament with $N_e \sim 10^{16} \text{ cm}^{-3}$) [37], this theory is no longer valid. Because in such a case, no two THz beams, emitted from any longitudinal positions of the filament, could be totally out-phase to achieve destructive interference. Thus, in the far field after the two-color filament, there would be no detectable THz ring with enough contrast.

Nevertheless, far-field THz rings have been detected from a two-color filament with only ~ 6 mm in length [16]. And the 1DND model has been suggested to interpret the observed THz profile with higher-frequency THz component in the inner ring [16]. The key point of 1DND model is associated with the propagation of THz wave inside the plasma column and diffraction at the end of the filament, similar with the physical process described in Section 2.3 of this work.

However, there are still many other reports cannot be satisfyingly explained by the off-axis phase matching or 1DND model. Some of them can be found in the references as shown in the last three rows of Table 2.

Although, the publications [32], [35], [37]–[43] in Table 2 have their own self-consistent theories, one unified mechanism is still in urgent need. Here, we suggest that the micro-cavity model of the filament may qualitatively account for the above experimental phenomena [32], [35], [37]–[43].

- I) As can be seen in Fig. 4(b), at the beginning part of the θ - f curves in low THz band, there is a positive correlation relationship between THz radiation angle θ and frequency f , which has also been observed in Ref. [32].
- II) Then, in the top-value area of θ - f distribution, one can see θ remains almost the same regardless of f variation, which might be the phenomenon reported in Ref. [41].
- III) Next, in the most part of θ - f evolution, clearly θ decreases with the increasing f . This is actually what is frequently observed in the literature [37]–[40].
- IV) Furthermore, as for the on-axis propagation ($\theta \sim 0$) of THz wave during two-color filamentation [35], [42], [43], the THz frequency content needs to be rather high, as demonstrated in Ref. [35]. This agrees with our calculation outcomes of θ - f in high THz band as shown in Fig. 4(b) where θ is close to 0 as well.

3. Experimental Verification

Although analytic calculations and FDTD simulations have been carried out in this work, it is still better to achieve experimental evidences of the existence of the plasma micro-cavity effect. Previously, it has been reported that one could experimentally observe the filament-guided propagation of THz pulses, which were injected from another filament, in case of crossing the two filaments from the same laser amplifier [47]. This indirectly proved the THz guiding effect induced by the plasma micro-cavity. Based on the same thought, we actually have ever tried focusing an air plasma-based THz beam into another filament channel (without filaments interaction) and detecting the modulated THz signal. However, the expected micro-cavity effect of the filament on the injected THz wave is not remarkable. This might be due to the huge difference of the spatial sizes between the filament

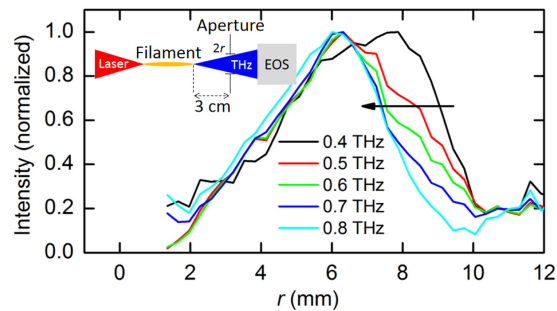


Fig. 8. Radial distributions of THz intensity as a function of r at five THz frequencies. The black arrow pointed out the variation trend to the higher-frequency THz component. Inset: the schematic of profiling the THz beam with an adjustable aperture and a traditional THz-EOS.

($\sim 100 \mu\text{m}$ in diameter) and the focused THz beam ($\sim 2 \text{ mm}$ in diameter). As for this issue, we have planned to achieve a sub-wavelength-scale THz beam, e.g., via super-resolution focusing by a metalens [48], [49], and then repeat the experiment. This work is still underway.

On the other hand, the proposed physical model in this work, as well as the following numerical simulations, have drawn a consistent conclusion on the frequency dependence of the spatial distribution of the THz emission from a laser filament. That is, the high-frequency content tends to be located in the inner ring of the circular cross section of the THz beam. On this aspect, an additional experiment has been carried out by using a 1 kHz (repetition frequency), 800 nm (central wavelength) and 50 fs (FWHM of the temporal width) Ti:sapphire laser pulse with 1 mJ/pulse. The laser pulse was focused by a $f = 100 \text{ cm}$ lens, creating a centimeter-scale long single-color filament in the air as the source of THz radiation. The detection setup was a traditional THz electro-optical sampling (EOS) system. Between the filament and the EOS setup, an adjustable aperture has been positioned with a distance of about 3 cm from the end of the filament, in order to characterize the emitted THz beam profile.

As shown as the inset in Fig. 8, varying the opening radius r of the aperture, the waveforms of transmitted THz pulses were recorded by the EOS setup. Next, via differential and Fourier transformations on the detected THz waveforms, the spectral intensity as a function of r at one certain THz frequency can be retrieved. Fig. 8 displays such radial distributions of THz spectral intensity at 0.4, 0.5, 0.6, 0.7 and 0.8 THz, respectively. Note that 0.6 THz was the peak frequency of the detected THz spectrum in our experiment.

It can be clearly seen that the THz intensity with higher frequency tends to be located at a smaller r (as pointed by the black arrow in Fig. 8), namely, the inner ring of the THz radiation profile. This is in agreement with our theoretical conclusion (Fig. 4, 6 and 7). Moreover, the detected radiation angle θ of the THz wave is about $\arctan(6 \text{ mm} / 3 \text{ cm}) = 12 \text{ degree}$ at 0.8 THz. Reading Fig. 4(b), similar information can also be obtained if assuming the mean N_e of the filament is 10^{15} cm^{-3} (the green line). This further proved the validity of our model.

4. Discussion

In this work, the proposed micro-cavity model might suffer the lack of more precise quantitative results, compared with thorough mathematical calculations based on theoretical physics, such as particle-in-cell (PIC) model [44]–[46]. However, the micro-cavity model could quickly provide physical explanations about the experimental results without going through time-consuming rigorous computational operations. For instance, Eq. (10) is able to tell immediately that the radiation angle of a THz wave in the far field after the filament decreases with the increasing THz frequency, which is a foresight with great guiding significance. In addition, Eq. (10) predicts $\theta \sim 0$ for rather high-frequency content of the THz emission. This has been experimentally confirmed by implementing an open pinhole in the THz beam path and observing the on-axis propagating THz mode [35].

5. Conclusion

In summary, in view of the radial step index distribution of a laser filament in the THz spectral region, the plasma channel is expected to be a micro-cavity for the created THz wave. In this case, the propagating THz wave could undergo multiple reflections and refractions at the interface between the filament and air. Consequently, both inside the plasma column and in the far field, the THz electric fields have been inferred to appear as ring modes with frequency dependence. This resonance waveguide model of the laser filament is helpful to shed light on the complicated THz profiles reported in the publications (please see Table 1 and 2). More importantly, it confirms the role of the filament plasma as a THz waveguide, which has already been experimentally demonstrated in other frequency bands, such as the microwave [50], [51], NIR and x-ray [18], [19], etc.

Appendix

The details of the derivation of Eq. (6) have been presented as follows. Firstly, in view of Fig. 3(b), the optical path difference Δ between two adjacent refracted THz beams is given by

$$\begin{aligned}
 \Delta &= n_{\text{THz}}(AB + BC) - n_{\text{air}}(AD) \\
 &= n_{\text{THz}}(2AB) - n_{\text{air}}(AC \sin \theta'') \\
 &= n_{\text{THz}}(2AB) - n_{\text{air}}(2AB \sin \theta' \sin \theta'') \\
 &= 2AB(n_{\text{THz}} - n_{\text{air}} \sin \theta' \sin \theta'') \\
 &= 2 \frac{d}{\cos \theta'} (n_{\text{THz}} - n_{\text{air}} \sin \theta' \sin \theta'') \tag{a1}
 \end{aligned}$$

At the interface between the plasma and air, the THz wave followed the Snell's law:

$$n_{\text{air}} \sin \theta'' = n_{\text{THz}} \sin \theta' \tag{a2}$$

which can be substituted into the equation of Δ , and one will obtain

$$\begin{aligned}
 \Delta &= 2 \frac{d}{\cos \theta'} (n_{\text{THz}} - n_{\text{THz}} \sin^2 \theta') \\
 &= 2 \frac{d}{\cos \theta'} n_{\text{THz}} (1 - \sin^2 \theta') \\
 &= 2 \frac{d}{\cos \theta'} n_{\text{THz}} \cos^2 \theta' \\
 &= 2n_{\text{THz}} d \cos \theta' \tag{a3}
 \end{aligned}$$

On the other hand, if considering the constructive coherence of THz waves in the far field, the optical path difference Δ should be an integral multiple (m) of the THz wavelength λ_{THz} , thus

$$\Delta = m\lambda_{\text{THz}} \tag{a4}$$

Hence, it is clear that

$$\begin{aligned}
 m\lambda_{\text{THz}} &= 2n_{\text{THz}} d \cos \theta' = 2n_{\text{THz}} d \sqrt{1 - \sin^2 \theta'} \\
 &= 2n_{\text{THz}} d \sqrt{1 - \left(\frac{n_{\text{air}} \sin \theta''}{n_{\text{THz}}} \right)^2} \\
 &= 2n_{\text{THz}} d \sqrt{1 - \left(\frac{n_{\text{air}} \cos \theta}{n_{\text{THz}}} \right)^2} (\because \theta'' + \theta = 90) \tag{a5}
 \end{aligned}$$

and thus

$$\begin{aligned}
 \cos \theta &= \frac{n_{\text{THz}}}{n_{\text{air}}} \sqrt{1 - \left(\frac{m\lambda_{\text{THz}}}{2n_{\text{THz}}d} \right)^2} \\
 &= \sqrt{\left(\frac{n_{\text{THz}}}{n_{\text{air}}} \right)^2 - \left(\frac{n_{\text{THz}}}{n_{\text{air}}} \frac{m\lambda_{\text{THz}}}{2n_{\text{THz}}d} \right)^2} \\
 &= \sqrt{\left(\frac{2n_{\text{THz}}d}{2n_{\text{air}}d} \right)^2 - \left(\frac{m\lambda_{\text{THz}}}{2n_{\text{air}}d} \right)^2} \\
 &= \sqrt{\frac{(2n_{\text{THz}}d)^2 - (m\lambda_{\text{THz}})^2}{(2n_{\text{air}}d)^2}} \tag{a6}
 \end{aligned}$$

This final outcome was written as Eq. (6) in the main text.

References

- [1] H. Hamster, A. Sullivan, S. Gordon, W. White, and R. W. Falcone, "Subpicosecond, electromagnetic pulses from intense laser-plasma interaction," *Phys. Rev. Lett.*, vol. 71, pp. 2725–2728, 1993.
- [2] C. C. Cheng, E. M. Wright, and J. V. Moloney, "Generation of electromagnetic pulses from plasma channels induced by femtosecond light strings," *Phys. Rev. Lett.*, vol. 87, pp. 213001-1–213001-4, 2001.
- [3] S. Tzortzakis *et al.*, "Coherent subterahertz radiation from femtosecond infrared filaments in air," *Opt. Lett.*, vol. 27, pp. 1944–1946, 2002.
- [4] G. Méchain, S. Tzortzakis, B. Prade, M. Franco, A. Mysyrowicz, and B. Leriche, "Calorimetric detection of THz radiation from femtosecond filaments in air," *Appl. Phys. B*, vol. 77, pp. 707–709, 2003.
- [5] C. D'Amico, A. Houard, M. Franco, B. Prade, and A. Mysyrowicz, "Coherent and incoherent radial THz radiation emission from femtosecond filaments in air," *Opt. Exp.*, vol. 15, pp. 15274–15279, 2007.
- [6] C. D'Amico *et al.*, "Conical forward THz emission from femtosecond-laser-beam filamentation in air," *Phys. Rev. Lett.*, vol. 98, pp. 235002-1–235002-4, 2007.
- [7] C. D'Amico *et al.*, "Forward THz radiation emission by femtosecond filamentation in gases: Theory and experiment," *New J. Phys.*, vol. 10, pp. 013015-1–013015-18, 2008.
- [8] H. C. Wu, J. Meyer-ter-Vehn, H. Ruhl, and Z. M. Sheng, "Terahertz radiation from a laser plasma filament," *Phys. Rev. E*, vol. 83, pp. 036407-1–036407-4, 2011.
- [9] Y. Minami, T. Kurihara, K. Yamaguchi, M. Nakajima, and T. Suemoto, "Longitudinal terahertz wave generation from an air plasma filament induced by a femtosecond laser," *Appl. Phys. Lett.*, vol. 102, pp. 151106-1–151106-3, 2013.
- [10] J. Zhao *et al.*, "Investigating the non-radially polarized component of terahertz wave emission during single-colour femtosecond laser filamentation in air," *J. Opt.*, vol. 20, pp. 105502-1–105502-10, 2018.
- [11] F. Jahangiri *et al.*, "Directional terahertz emission from air plasma generated by linearly polarized intense femtosecond laser pulses," *Appl. Phys. Exp.*, vol. 5, pp. 026201-1–026201-3, 2012.
- [12] F. Jahangiri, M. Hashida, S. Tokita, T. Nagashima, M. Hangyo, and S. Sakabe, "Enhancing the energy of terahertz radiation from plasma produced by intense femtosecond laser pulses," *Appl. Phys. Lett.*, vol. 102, pp. 191106-1–191106-4, 2013.
- [13] A. Debayle, L. Gremillet, L. Bergé, and C. Köhler, "Analytical model for THz emissions induced by laser-gas interaction," *Opt. Exp.*, vol. 22, pp. 13691–13709, 2014.
- [14] P. Sprangle, J. R. Penano, B. Hafizi, and C. A. Kapetanakos, "Ultrashort laser pulses and electromagnetic pulse generation in air and on dielectric surfaces," *Phys. Rev. E*, vol. 69, pp. 066415-1–066415-18, 2004.
- [15] E. Cabrera-Granado, Y. Chen, I. Babushkin, L. Bergé, and S. Skupin, "Spectral self-action of THz emission from ionizing two-color laser pulses in gases," *New J. Phys.*, vol. 17, pp. 023060-1–023060-9, 2015.
- [16] J. Zhao *et al.*, "Strong spatial confinement of terahertz wave inside femtosecond laser filament," *ACS Photon.*, vol. 3, pp. 2338–2343, 2016.
- [17] J. Zhao *et al.*, "Clue to a thorough understanding of terahertz pulse generation by femtosecond laser filamentation," *Photon. Res.*, vol. 6, pp. 296–306, 2018.
- [18] J. Zhao *et al.*, "Propagation of terahertz wave inside femtosecond laser filament in air," *Laser Phys. Lett.*, vol. 11, pp. 095302-1–095302-6, 2014.
- [19] B. Zeng *et al.*, "Enhancement of peak intensity in a filament core with spatiotemporally focused femtosecond laser pulses," *Phys. Rev. A*, vol. 84, pp. 063819-1–063819-7, 2011.
- [20] Y. H. Chen, S. Varma, T. M. Antonsen, and H. M. Milchberg, "Direct measurement of the electron density of extended femtosecond laser pulse-induced filaments," *Phys. Rev. Lett.*, vol. 105, pp. 215005-1–215005-4, 2010.
- [21] H. M. Milchberg, T. R. Clark, C. G. Durfee, III, T. M. Antonsen, and P. Mora, "Development and applications of a plasma waveguide for intense laser pulses," *Phys. Plasmas*, vol. 3, pp. 2149–2155, 1996.
- [22] C. G. Durfee, III and H. M. Milchberg, "Light pipe for high intensity laser pulses," *Phys. Rev. Lett.*, vol. 71, pp. 2409–2412, 1993.

- [23] A. Houard, Y. Liu, B. Prade, V. T. Tikhonchuk, and A. Mysyrowicz, "Strong enhancement of terahertz radiation from laser filaments in air by a static electric field," *Phys. Rev. Lett.*, vol. 100, pp. 255006-1–255006-4, 2008.
- [24] G. Dutier, S. Saltiel, D. Bloch, and M. Ducloy, "Revisiting optical spectroscopy in a thin vapor cell: Mixing of reflection and transmission as a Fabry–Perot microcavity effect," *J. Opt. Soc. Amer. B*, vol. 20, pp. 793–800, 2003.
- [25] D. G. Guo, R. M. Lin, and W. J. Wang, "Modelling and optimization of a Fabry–Perot microcavity for sensing applications," *J. Opt.*, vol. 6, pp. 1027–1035, 2004.
- [26] C. Köhler, E. Cabrera-Granado, I. Babushkin, L. Bergé, J. Herrmann, and S. Skupin, "Directionality of terahertz emission from photoinduced gas plasmas," *Opt. Lett.*, vol. 36, pp. 3166–3168, 2011.
- [27] J. Zhao *et al.*, "Terahertz imaging with sub-wavelength resolution by femtosecond laser filament in air," *Sci. Rep.*, vol. 4, pp. 3880-1–3880-7, 2014.
- [28] K. Y. Kim, J. H. Glowina, A. J. Taylor, and G. Rodriguez, "Terahertz emission from ultrafast ionizing air in symmetry-broken laser fields," *Opt. Exp.*, vol. 15, pp. 4577–4584, 2007.
- [29] A. Couairon and A. Mysyrowicz, "Femtosecond filamentation in transparent media," *Phys. Rep.*, vol. 441, pp. 47–189, 2007.
- [30] B. E. Saleh, M. C. Teich, and B. E. Saleh, *Fundamentals of Photonics*. Hoboken, NJ, USA: Wiley, 1991.
- [31] F. Théberge, W. Liu, P. T. Simard, A. Becker, and S. L. Chin, "Plasma density inside a femtosecond laser filament in air: Strong dependence on external focusing," *Phys. Rev. E*, vol. 74, pp. 036406-1–036406-7, 2006.
- [32] H. Zhong, N. Karpowicz, and X. C. Zhang, "Terahertz emission profile from laser-induced air plasma," *Appl. Phys. Lett.*, vol. 88, pp. 261103-1–261103-3, 2006.
- [33] P. G. de Alaiza Martínez, X. Davoine, A. Debayle, L. Gremillet, and L. Bergé, "Terahertz radiation driven by two-color laser pulses at near-relativistic intensities: Competition between photoionization and wakefield effects," *Sci. Rep.*, vol. 6, pp. 26743-1–26743-14, 2016.
- [34] C. Miao, J. P. Palastro, and T. M. Antonsen, "Laser pulse driven terahertz generation via resonant transition radiation in inhomogeneous plasmas," *Phys. Plasmas*, vol. 23, pp. 063103-1–063103-11, 2016.
- [35] P. Klarskov and P. U. Jepsen, "Observation of forward propagating THz mode emitted from a two-color laser-induced air plasma," *J. Infrared Millimeter THz Waves*, vol. 34, pp. 777–779, 2013.
- [36] D. J. Cook and R. M. Hochstrasser, "Intense terahertz pulses by four-wave rectification in air," *Opt. Lett.*, vol. 25, pp. 1210–1212, 2000.
- [37] Y. S. You, T. I. Oh, and K. Y. Kim, "Off-axis phase-matched terahertz emission from two-color laser-induced plasma filaments," *Phys. Rev. Lett.*, vol. 109, pp. 183902-1–183902-5, 2012.
- [38] A. Gorodetsky, A. D. Koulouklidis, M. Massaouti, and S. Tzortzakis, "Physics of the conical broadband terahertz emission from two-color laser-induced plasma filaments," *Phys. Rev. A*, vol. 89, pp. 033838-1–033838-6, 2014.
- [39] V. Blank, M. D. Thomson, and H. G. Roskos, "Spatio-spectral characteristics of ultra-broadband THz emission from two-colour photoexcited gas plasmas and their impact for nonlinear spectroscopy," *New J. Phys.*, vol. 15, pp. 075023-1–075023-20, 2013.
- [40] P. Klarskov, A. C. Strikwerda, K. Iwaszczuk, and P. U. Jepsen, "Experimental three-dimensional beam profiling and modeling of a terahertz beam generated from a two-color air plasma," *New J. Phys.*, vol. 15, pp. 075012-1–075012-13, 2013.
- [41] P. Klarskov, M. Zalkovskij, A. C. Strikwerda, and P. U. Jepsen, "Spectrally resolved measurements of the terahertz beam profile generated from a two-color air plasma," in *Proc. Conf. Lasers Electro-Opt.*, 2014, Paper STu1F-6.
- [42] A. D. Koulouklidis, M. Massaouti, A. Gorodetsky, and S. Tzortzakis, "Understanding and controlling on-axis and off-axis THz emission patterns from 2-color femtosecond laser filaments," in *Proc. Eur. Conf. Lasers Electro-Opt. Eur./Int. Quantum Electron. Conf.*, 2013, Paper CC_P_14.
- [43] P. Klarskov, T. Wang, J. D. Buron, A. C. Strikwerda, and P. U. Jepsen, "Spatial properties of a terahertz beam generated from a two-color air plasma," *Proc. SPIE*, vol. 8846, 2013, Art. no. 88460R.
- [44] Z. M. Sheng, K. Mima, J. Zhang, and H. Sanuki, "Emission of electromagnetic pulses from laser wakefields through linear mode conversion," *Phys. Rev. Lett.*, vol. 94, pp. 095003-1–095003-4, 2005.
- [45] W. M. Wang, P. Gibbon, Z. M. Sheng, and Y. T. Li, "Tunable circularly polarized terahertz radiation from magnetized gas plasma," *Phys. Rev. Lett.*, vol. 114, pp. 253901-1–253901-5, 2015.
- [46] W. M. Wang, Z. M. Sheng, H. C. Wu, M. Chen, and K. Mima, "Strong terahertz pulse generation by chirped laser pulses in tenuous gases," *Opt. Exp.*, vol. 16, pp. 16999–17006, 2008.
- [47] H. W. Du, H. Hoshina, C. Otani, and K. Midorikawa, "Terahertz waves radiated from two noncollinear femtosecond plasma filaments," *Appl. Phys. Lett.*, vol. 107, pp. 211113-1–211113-4, 2015.
- [48] L. Dylan and Z. Liu, "Hyperlenses and metalenses for far-field super-resolution imaging," *Nature Commun.*, vol. 3, pp. 1205-1–1205-9, 2012.
- [49] C. Ma and Z. Liu, "A super resolution metalens with phase compensation mechanism," *Appl. Phys. Lett.*, vol. 96, pp. 183103-1–183103-3, 2010.
- [50] M. Alshershby, Y. Ren, J. Qin, Z. Hao, and J. Lin, "Diagnosis of femtosecond plasma filament by channeling microwaves along the filament," *Appl. Phys. Lett.*, vol. 102, pp. 204101-1–204101-4, 2013.
- [51] Y. Ren, M. Alshershby, J. Qin, Z. Hao, and J. Lin, "Microwave guiding in air along single femtosecond laser filament," *J. Appl. Phys.*, vol. 113, pp. 094904-1–094904-5, 2013.